Master's Thesis of Science

in Agricultural Biotechnology

Colon-targeted and sustained release of curcumin using chitosan-coated alginate-pectin beads with internal egg-box structure

대장에서 지속적인 커큐민의 방출을 위한 내부적 달걀 상자 구조를 유도한 키토산 코팅된 알긴산-펙틴 환

August, 2021

The Graduate School

Seoul National University

Department of Agricultural Biotechnology

Yang, Ji Soo

석사학위논문

Colon-targeted and sustained release of curcumin using chitosan-coated alginate-pectin beads with internal egg-box structure

지도교수 최 영 진

이 논문을 석사학위 논문으로 제출함

2021년 8월

서울대학교 대학원

농 생 명 공 학 부

양 지 수

양지수의 석사 학위논문을 인준함

2021년 8월

위원장 유 상 열

부위원장 최 영 진

위원 하 남 출

CONTENTS

LIST OF TABLES

LIST OF FIGURES

ABSTRACT

Curcumin has anti-inflammatory and anti-cancer effects in the colon. However, it has low bioavailability due to its low water solubility and stability. To overcome the limitations, hydrogel beads were made of sodium alginate (SA) and low methoxyl pectin (LMP), which were not decomposed by digestive enzymes and had pH-sensitive properties. The beads were manufactured by ionic-interaction of COO^- of SA/LMP with NH_3^+ of chitosan, and by crosslinking with Ca^{2+}. Due to the large porosity of SA and the weak textural properties of LMP, the beads made of only SA and LMP respectively caused the burst release of core substance. Therefore, the beads were prepared by physical entanglement of SA and LMP, and formation of egg-box structure through internal gelation (IG), resulting in uniform and denser structure. The results of FTIR indicated the cross-linking between carboxylic acid of SA/LMP and calcium ions, and the polyelectrolyte complex between carboxylic acid of SA/LMP and NH_3^+ of CS. Also, the XRD analysis represented that IG induced more regular structure and high crystallinity. The beads were stable in gastric pH, and they were dissolved in small intestinal pH due to higher pKa, and degraded by pectinase in simulated large

intestinal fluid (pH 7.4). The compact and uniform structures of the beads with IG prevented severe burst release in small intestinal pH and induced sustained release in large intestinal fluid. In the case of 2:1 blend of SA/LMP without IG, about 29% of curcumin was released in small intestinal pH and 80% in simulated large intestinal fluid in 2 h. The beads with IG released only 14% in small intestinal pH and 80% in simulated large intestinal fluid in 5 h. These results indicated that the formation of egg-box structure through IG prevented burst release in small intestinal pH and induced sustained release in simulated large intestinal fluid.

Keywords : hydrogel beads; sodium alginate; low methoxyl pectin; chitosan-coating; internal gelation; egg-box structure; external gelation; polyelectrolyte complex; colon-targeted release

I. Introduction

Bioactive phytochemicals, which are derived from various natural sources such as plants, fruits, and vegetables, possess diverse bioactivity in the colon, including inhibition of colon cancer, reduction of inflammation, promotion of the growth of probiotics (Kun Feng, 2020), thus they benefit colon health. Especially, curcumin exhibits anticancer and anti-inflammatory properties. Current studies indicate that curcumin can inhibit the proliferation of colon cancer cells and effectively mitigate ulcerative colitis (B. B. Patel et al., 2009). Curcumin has been noticed to have properties to inhibit a growth of colon cancer, and induce apoptosis in colon cancer cells of which use could be a potentially promising approach for cancer therapy (Sookka et al., 2015). However, the clinical application of curcumin is limited by its low oral bioavailability, which is caused by poor water solubility. Moreover, curcumin has a short half-life and less active metabolites. Thus, delivery systems that can improve curcumin solubility and achieve sustained release are highly valuable. In order to enhance the effect of curcumin in colon, the oral colon specific delivery system that can directly carry curcumin to colon and release curcumin with high concentration in colon has been developed.

The alginate polymer is composed of linear chains of α-L-guluronic acid (G) and β-D-mannuronic acid (M) blocks identified as rigid and flexible blocks, respectively (S.N. Pawar, K.J. Edgar, 2012). The fast degradation and rapid dissolution of alginate matrices in the higher pH ranges may result in burst release of core materials (M.George, T.E. Abraham, 2006; Lee K.Y., 2012). Likewise, the major limitation of Ca-alginate beads is the loss of functional substance during bead preparation, by leaching through the pores in the beads (P. Liu, 1999; M.L. Torre, 1998). Moreover, the relatively large pore size of alginate, and the physical instability of alginate in higher pH media resulted in burst release of functional substance. However, alginates possess several advantages as colon-specific carriers, including pH sensitivity, high adherence to the colonic mucosa, and colonic microflora-catered biodegradability.

Pectin-based hydrogels are not degraded in the stomach and consequently can protect the loaded compound. Low methoxyl pectin, low methyl-esterified pectin with degree of esterification less than 50% can interact with calcium ions or multivalent cations that cross-link the galacturonic acid chains and finally form gels. However, they are easily swelling and disintegrated in the small intestine because of their low

calcium sensitivity and low rheological properties (Günter, E. A., & Popeyko, O. V., 2016). In other words, they could not deliver the functional substances such as phytochemicals to the colon successfully. Therefore, through combination of alginate and pectin, it could prevent the burst release of alginate in small intestine and colon, and delayed the burst disintegration of the pectin by the pectinase. In the previous studies, the controlled beads based on alginate, pectin, and glutaraldehyde increased retard release of curcumin in the stomach and small intestine, while admitting complete release in colon (N. Sattarahmady et al, 2016), and the Eudragit S100-caoted alginate/pectin beads were developed for sustained release of core substance for colon-targeted delivery (F.-Y. Hsu, 2013).

The main limitation of chitosan for delivery is the easy dissolution of chitosan in the low pH of stomach (Martău, G.A., 2019). The easy solubility of chitosan in low pH is prevented by the formation of polyelectrolyte complex with alginate and pectin, since alginate is insoluble in low pH conditions. Also, the possible dissolution of alginate and pectin at higher pH is prevented by the chitosan which is stable at higher pH ranges. In other words, alginate/pectin and chitosan can form polyelectrolyte complex (PEC) together by ionic interaction via the

carboxyl residues of alginate and pectin, and amino groups of chitosan. Compared with hydrogel beads prepared with chitosan alone, the PEC beads possess physicochemical properties, such as enhanced stability in swelling media of different pH, improved structural strength and mechanical stability (M. Gierszewska, 2018; Y. Luo, 2014). The complex coacervation of oppositely charged polyelectrolytes has been extensively used to prepare and strengthen alginate and pectin particles (M. Leonard, 2004). Moreover, the additional coating of hydrogels with oppositely charged substances can offer a diffusion barrier to delay rapid release in well-controlled delivery systems (Jeddi & Mahkam, 2019; Rafi & Mahkam, 2015). In acid conditions, chitosan remains soluble and can form a thick swollen layer, which acts as a diffusional barrier for the release of core material (Kampanart Huanbutta et al., 2013). The phenomenon was considered to correlate with the polyelectrolyte complexation between positively charged amino groups of chitosan and the carboxylic residues of the alginate and pectin, which enhanced the stability of hydrogel.

To form egg-box structures through internal gelation (IG), the GDL which slowly hydrolyzes in aqueous solution forming glucuronic acid of alginate and galacturonic acid of pectin resulted in a slow release

of calcium ions inducing and forming homogeneous gels. (P. Jantrawut et al., 2013; D. Rajmohan, 2019). So far, attempts to induce IG have been conducted using pectin beads depending on the presence of IG, which increased entrapment of core substance (A. P. Pawar et al., 2008), and alginate emulsion microspheres with controlled amount of $CaCO_3$ inducing IG for delivery of bifidum (Q. Zou et al., 2011), while chitosan-coated alginate/pectin hydrogel beads with controlled internal egg-box structure have not been used so far as a colon-targeted delivery system of curcumin.

A variety of polysaccharides, like low-methoxyl pectin, alginate, and chitosan which were used in this study, have been used to produce hydrogel beads for delivery systems because of their good biocompatibility, biodegradability, and non-toxicity (Gadalla, El-Gibaly, Soliman, Mohamed, & El-Sayed, 2016; Maitra & Shukla, 2014). In this study, I hypothesized that the controlled degree of IG depending on the mixing ratio SA and LMP could be used to CS-coated beads suitable for sustained releasing of colon-targeted curcumin, resulting in more stable networks. I controlled the degree of IG applied to blended suspension composed of SA/LMP which can be delivery beads formed by external gelation (EG). To overcome the drawbacks of the alginate beads like

porosity and burst release, and pectin beads like low textural properties, the beads were formed by physical entanglement of SA and LMP, and coated with CS that led to the formation of polyelectrolyte complexes through inter-ionic interactions between oppositely charged biopolymers. The hydrogel beads were characterized by XRD, FTIR and SEM to study their interactions and structures. In addition, the releasing behavior of curcumin in the beads were observed.

II. Materials and methods

2.1. Materials

Sodium alginate and pectin from citrus peel (galacturonic acid ≥74.0 %) were purchased from Sigma Aldrich. Curcumin was purchased from ACROS, and Glucono-Delta-Lactone (GDL) from esfood (Gunpo, Korea), and calcium carbonate from JUNSEI. Chitosan (5-20 mPa·s) was purchased from TCI, and calcium chloride (dehydrate) from DUKSAN.

2.2. Gel preparation and rheological measurements

The gels were prepared by dissolving SA/LMP in D.W. (0.3 g/10 mL) using high magnetic stirring. To form internal gelation (IG) inducing egg-box structure, $CaCO_3$ was then added for 1 min under 1200 rpm, followed by glucono delta lactone (GDL) for 5 min under 900 rpm. The GDL which slowly hydrolyzes in aqueous solution forming gluconic acid resulted in a slow release of calcium ions inducing and forming gels (P. Jantrawut et al., 2013).

SA : LMP	2:1	1:1	1:2
$CaCO_3$ (g)	0.005	0.045	0.003
GDL (g)	0.035	0.0315	0.021

The cross-linking solution was composed of CS 0.8% and $CaCl_2$ 2%. To form external gelation, the solution or the gels formed by IG were dropped into the cross-linking solution (10 mL/40 mL). The hydrogel beads were dried overnight in 40°C dry oven to be dried beads.

The rheological behavior of gels formed by IG were investigated using the rheometer (HAAKE RheoStress 1). The oscillatory frequency sweep tests were performed over the angular frequency range from 0.01 to 1 Hz at 25°C. The shear stress amplitude was fixed at 1 Pa. A parallel plate shape made of stainless steel (diameter 20 mm) was selected. The storage modulus (G*'*), loss modulus (G*''*), and complex viscosity (η*), were determined as functions of frequency.

2.3. Measurement of particle size

Particle size was measured using the image processing software Image J. The smallest and largest diameters of each particle were measured, and the diameter was expressed as a mean of them (G.L.A. Sampaio, et al., 2019).

2.4. Texture profile analysis (TPA)

The samples used for Texture profile analysis (TPA) were prepared by the procedure of preparation of gel samples. Texture profile analysis was carried out at room temperature (apporoximately 20°C). The samples were penetrated with a TA11/1000 probe. The sample was compressed twice at a deformation of 40% sample height and a speed of 1 mm/s with control force of 5 g-force, and textural parameters, including hardness and springiness were recorded.

2.5. X-ray diffraction (XRD)

The X-ray diffraction pattern of the samples was verified with a D8 ADVANCE with DAVINCI (BRUKER, German) using Cu Kα1 radiation at 40 kV, 40mA in the scan range of 2 θ from 5 to 60◦, step : 0.02, scan speed : 1 sec/step (= 1.5418Å).

2.6. Fourier transform infrared spectroscopy (FT-IR)

FTIR spectral analysis was done using Nicolet 6700 (Thermo Scientific, USA) with a scan range of 600–4000 cm^{-1} to confirm the compatibility of different ingredients of the formulation.

2.7. Scanning electron microscopy (SEM) observation

Before observation, compound gels were lyophilized by a vacuum freeze dryer at -40°C. The samples were fixed on a microscope stub, and then coated with platinum layer (15 nm thickness). The samples were observed by SEM with a potential accelerator of 2 kV and magnified 100× and 200× times.

2.8. Releasing behavior

Phosphate-Buffered Saline (PBS, 1×, pH 7.4) was used to adjust pH of small intestine and large intestine (colon). 100 mg beads were weighed and added to 40 mL of fluid depending on pH of gastro (pH 2 for 2 h), small intestine (pH 6.8 with PBS for 3 h), and colon (pH 7.4, PBS) consecutively at 37℃ under 60 rpm. Samples (0.5 mL) were withdrawn every 30 minutes in pH 6.8 and pH 7.4. In pH 7.4 fluid imitating colon, the enzyme, which is pectinase, was added to evaluate the release profiles of embedded components. The addition of Pectinex (3 mL/L) serves to mimic the enzymes generated by the microorganisms present in the colon, hence, the enzyme enriched simulation media are often viewed as an effective way of evaluating the release profiles of different colon targeted vehicles, especially for those based on microflora activated mechanisms.

Absorbance measurement at 426 nm allowed quantifying the amount of released curcumin using the calibration curve. Then the percentage of curcumin released was determined and plotted over time. All experiments were performed in triplicate (A.T.-B. Nguyen et al., 2014).

Release (%) = Released curcumin / Total curcumin in beads × 100

2.9. Statistical analyses

Statistical analysis of the results was performed using a Statistical Package for the Social Sciences System (SPSS Statistics 25). Duncan's multiple range test was used to identify significant differences ($P < 0.05$) between means. The results were reported as mean ± standard deviation.

III. Results and discussion

3.1. Gel preparation and rheological properties of weak-gel induced by internal gelation (IG)

In this study, the CS-SA/LMP hydrogel beads with different proportions of SA/LMP (2:1, 1:1, 1:2) and different extents of IG for colon-targeted curcumin delivery system were prepared by an egg-box model (internal gelation, IG) and ionic gelation (external gelation, EG) method. Since SA and LMP are negatively charged by carboxylic acid in the molecule, it can interact with positively charged substances. The amounts of non-esterified carboxyl groups (-COOH) in LMP were higher than high methoxyl pectin. Therefore, the hydrogel beads were successfully formed when the hydrogel beads were prepared by using LMP.

When GDL was added into the LMP solution containing $CaCO_3$, calcium ions were released and the gels were obtained by ionotropic gelation mechanism in which intramolecular crosslinks were formed between the negatively charged carboxyl groups of LMP and the positively charged counter ion (Ca^{2+}). The GDL and $CaCO_3$ were selected for use of the gel preparation method in order to slow down the formation and achieve a homogeneous gel (Pensak. J., 2013).

Curcumin was physically adsorbed on the beads. The hydrogen interaction between hydroxyl groups from curcumin and carboxyl groups of SA/LMP. Besides, curcumin had low water solubility and fast encapsulation of core material, thus the particels had high entrapment efficiency.

The effects of Ca^{2+} concentration on the gelation of alginate and pectin are mostly described as the R value (2 $[Ca^{2+}]/[COO^{-}]$), rather than the overall Ca^{2+} concentration (Fang et al., 2007). For both Ca-alginate and Ca-pectin gels, before reaching their saturated R values (0.55 for alginate and 0.3 for pectin), an increase in the Ca^{2+} concentration resulted in a fast gelation and a high strength, stiffness, and viscosity of the gels, because high concentration of Ca^{2+} led to a fast ion diffusion which promoted the formation of mono-complexes and egg-box dimers, generating a dense and elastic gel structure (L. Cao, et al., 2020). Therefore, alginate requires more amount of calcium ions, when there were the same amount of carboxyl groups of SA and LMP.

Elastic behavior of a hydrogel plays a leading role in maintaining its stable structure rather than the viscous behavior (X. Chen, 2019). It was noticed that the elastic properties of polymer formulations increased

with increasing the degree of IG in formulations. The beads including 2:1, 1:1, and 1:2 blend ratio of SA : LMP showed the same values of G', even if the amount of calcium ions used to induce IG was different (Fig. 1). Besides, all gels indicated that G' > G'', meaning that elastic properties was dominant than viscous properties and all gels had a comparatively stable network because of egg-box structure. As shown in Fig. 1, all the gels changed rapidly depending on increase of frequency, owing to weaker network structures. Therefore, all the gels were weak-gel and showed similar viscoelastic properties. Excessive formation of egg-box structure led to more little amount of carboxyl groups to form external gelation, resulting in irregular-shaped beads. As a result, the degree of IG, forming egg-box structure, should be controlled by the blend ratios of SA and LMP.

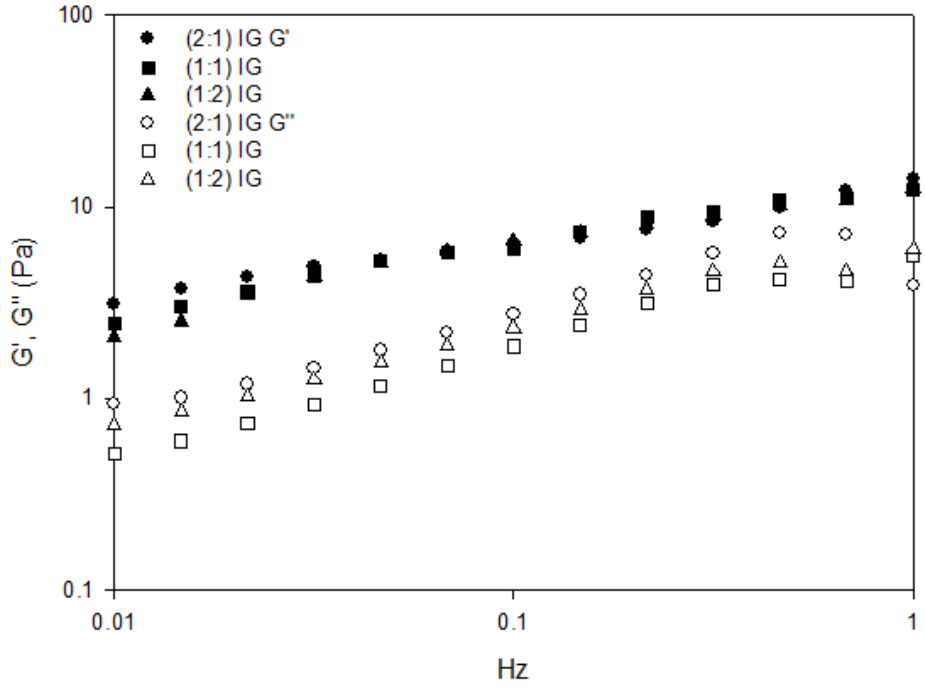

Figure 1. Rheological properties (G', G'') of suspension with internal gelation (IG) and different blend ratio of SA/LMP.

3.2. Appearance and particle sizes of beads

The hydrogel beads manufactured with higher proportions of SA showed a more circular and homogeneous shape (Fig. 2.). This is because there were more carboxylate groups in SA, therefore SA is more sensitive to calcium ions than LMP. SA could react more with calcium ion than LMP because of more presence of carboxylic acid.

The diameter of the hydrogel and dried beads developed by external ionotropic gelation are presented in Table. 1, respectively. The proper concentration of SA/LMP (3% w/v) and CS/$CaCl_2$ (0.8% w/v, 2% w/v, respectively) could provide uniform bead formation, except 5% concentration of LMP. LMP had much lower amount of carboxylate groups than SA, resulting in higher concentration required to manufacture the LMP beads. Although high concentration of LMP, the bead appeared to be irregular shape and the biggest size in both hydrogel and dried beads. Not only the beads manufactured with higher proportions of SA showed a regular and circular shape, but also the size of the beads were smaller than the beads with higher ratios of LMP (Table. 1). The higher SA ratios of the beads, the smaller the size of beads tended to be, even if there was no significant difference. SA beads and (2:1) EG beads evidently formed the smallest hydrogel and dried beads

with diameter about 3.0 mm and 1.19 mm, respectively. This is because there were more carboxylate groups which could interact with CS/Ca^{2+} on the bead surface in the beads with higher amount of SA.

The hydrogel beads were ranged from 2.995 to 3.720 mm. The sizes of (2:1), (1:1), and (1:2) EG hydrogel beads with only EG were 3.227, 3.319, and 3.587 mm, respectively. On the other sides, the sizes of (2:1), (1:1), and (1:2) IG hydrogel beads with both IG and EG were 3.011, 3.240, and 3.540 mm. The hydrogel beads with both IG and EG were smaller in size than the beads of the same blend ratios with only EG, although there was no significant difference. This might be related to the lower amount of carboxyl groups which could interact with CS and Ca^{2+} on the bead surface through surface-crosslinking (EG), because the carboxyl groups already formed egg-box structures through core-crosslinking (IG) in the beads. Therefore, the beads with IG induced lower amount of CS-coating through surface-crosslinking, resulting in smaller sizes of the beads.

The dried beads showed a significant decrease in diameter and they were ranged from 1.186 to 1.476 mm except LMP beads. Likewise, in dried beads, the beads with both core and surface-crosslinking showed smaller sizes than the beads with only surface-crosslinking. The size of

(2:1), (1:1), and (1:2) beads with only EG were ranged from 1.274 to 1.476 mm, but the beads with both IG and EG were ranged from 1.186 to 1.467 mm. The size of beads is an important factor of stability and reactivity of food in solutions, since Food and Drug Administraion (FDA) published the appropriate maximal bead size as 2.8 mm (10% variation of the target, ~2.5 mm) based on chewing and swallowing particle size, accordingly, the resulted dried beads in this study were well established (FDA, 2012).

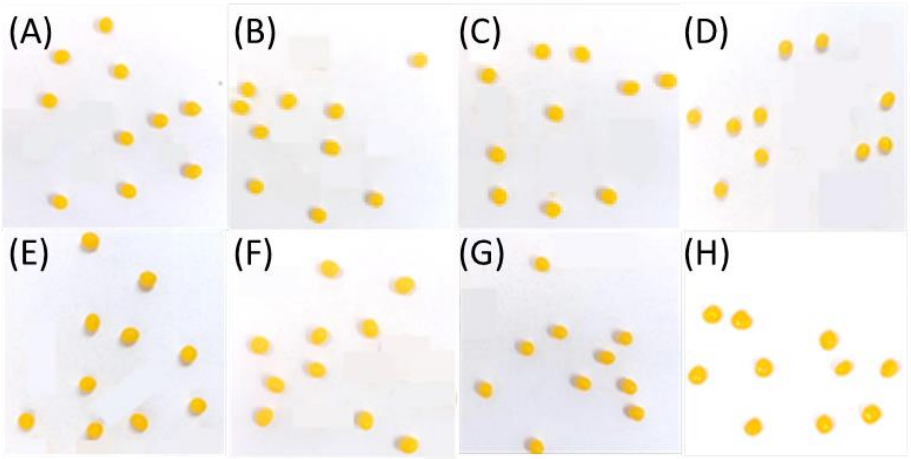

Figure 2. Appearance of the hydrogel beads depending on the presence of internal gelation (IG) and blend ratio of SA/LMP including (A) (2:1) EG (B) (2:1) IG (C) (1:1) EG (D) (1:1) IG (E) (1:2) EG (F) (1:2) IG (G) SA EG (H) LMP EG.

Table 1. Particle sizes of hydrogel and dried beads with different blend ratio of SA/LMP depending on the presence of internal gelation (IG)

	SA: LMP	Hydrogel beads (mm)	Dried beads (mm)
Only EG	2:1 CS	3.227 ± 0.169^{b}	1.274 ± 0.075^{ab}
	1:1 CS	3.319 ± 0.145^{b}	1.419 ± 0.031^{ab}
	1:1 Ca	3.360 ± 0.134^{b}	1.330 ± 0.055^{ab}
	1:2 CS	3.587 ± 0.164^{cd}	1.476 ± 0.065^{b}
	SA 3% CS	2.995 ± 0.139^{a}	1.196 ± 0.018^{a}
	LMP 5% CS	3.720 ± 0.232^{d}	2.483 ± 0.210^{c}
Both IG and EG	2:1 CS	3.011 ± 0.173^{a}	1.186 ± 0.067^{a}
	1:1 CS	3.240 ± 0.152^{b}	1.345 ± 0.002^{ab}
	1:2 CS	3.540 ± 0.187^{c}	1.467 ± 0.112^{b}

Values expressed are mean ± standard deviation. Data of different alphabets in the same column were different with statistical significant (p <0.05).

3.3. Texture profile analysis (TPA)

Mechanical strength and elasticity are the most critical features of the hydrogels used as a carrier system (X. Chen, 2019). The difference of the rigidity of gels could affect the percentage of swelling of the beads (Jantrawut et al., 2013). Also, beads with high elasticity and high mechanical strength are desirable for the sustained delivery purpose. Polymeric formulations with good elastic property maintain the stable structure of beads and facilitate the prolonged release of encapsulated compounds (A. Apoorva, 2020). The rigidity and elasticity of various gel formulations were evaluated as parameters of hardness and springiness index. The textural properties and swelling capacity could have an influence on the releasing pattern of beads.

The higher the SA ratio of SA/LMP beads, the stronger the textural properties (Table. 2). The SA had thicker wall, and more carboxyl groups which could cross-link with calcium ions at the bead surface than LMP, therefore SA beads showed higher rigidity and springiness. Thus, the higher SA proportions of the beads, the harder the beads tended to be. The hardness value of (2:1) EG beads and SA beads were 0.530 g_f, and 0.483 g_f, respectively. The higher hardness of (2:1) EG beads could be related to the physical entanglement of SA and LMP.

Moreover, the chain entanglement may increase the hydrophobic interactions in the beads. Whereas, springiness index was the highest values in SA beads.

The hardness of (1:1) CS beads which was coated by CS showed higher hardness (0.499 g_f) than (1:1) Ca beads (0.436 g_f) which was formed by only calcium ions through external gelation. The carboxyl groups of SA/LMP formed ionic-interaction with CS, and cross-linking with calcium ions. Therefore, the CS-coated (1:1) beads exhibited significantly stronger texture than the beads with only calcium-crosslinking, but similar springiness. CS polymers strengthened the textural properties of the beads.

The beads with both IG and EG showed lower values of hardness than the beads of the same blend proportions only with EG, even though there was no significant difference in (2:1) and (1:1) beads. In the case of (1:2) beads, the beads with IG and EG showed 0.421 g_f of hardness value, however the beads with only EG showed significantly lower hardness, 0.360 g_f. This is because the carboxyl groups of SA/LMP was used in formation of egg-box structure through IG, instead of more surface cross-linking with calcium ions and ionic-interaction with CS through EG, resulting in softer texture of the beads.

Table 2. Texture profile analysis of hydrogel beads with different blend ratio of SA/LMP depending on the presence of internal gelation (IG)

		Textural parameters		
	SA : LMP	Hardness 1 (gf)	Hardness 2 (gf)	Springiness index
Only EG	2:1 CS	0.530±0.002^{d}	0.446±0.006^{d}	0.532±0.033^{cd}
	1:1 CS	0.499±0.044^{cd}	0.429±0.030^{cd}	0.519±0.011^{cd}
	1:2 CS	0.421±0.027^{bc}	0.368±0.028^{c}	0.463±0.039^{bc}
	SA CS	0.483±0.027^{cd}	0.393±0.024^{cd}	0.546±0.013^{d}
	LMP CS	0.105±0.011^{a}	0.056±0.020^{a}	0.033±0.048^{a}
	1:1 Ca	0.436±0.013^{bc}	0.374±0.020^{c}	0.510±0.023^{cd}
Both IG and EG	2:1 CS	0.522±0.014^{d}	0.429±0.001^{cd}	0.528±0.001^{cd}
	1:1 CS	0.478±0.011^{cd}	0.405±0.012^{cd}	0.490±0.006^{cd}
	1:2 CS	0.360±0.016^{b}	0.289±0.016^{b}	0.394±0.009^{b}

Values expressed are mean ± standard deviation. Data of different alphabets in the same column were different with statistical significant (p <0.05).

3.4. X-ray diffraction (XRD)

X-ray diffraction studies provide the crystalline or amorphous nature of the core material in the polymer matrix. The XRD patterns of pure curcumin, CS, $CaCl_2$, SA, LMP, (1:1) of SA/LMP powder, (1:1) suspension powder, (1:1) IG suspension powder, Ca cross-linked (1:1) EG beads, CS-coated (1:1) EG beads, and CS-coated (1:1) IG beads are represented in Fig. 3.

The XRD patterns of sodium alginate showed in Fig. 4. The two peaks in XRD sepctra of SA exhibited at angles $2\theta = 13.85°$ and 21.75°, indicating polyguluronate and polymannuronate units of SA, respectively. Sodium alginate is usually crystalline due to strong interaction between the alginate chains through intermolecular hydrogen bonding (Fang, D., 2011). A similar result was observed by Fabia, J., (2005), who reported that three diffraction peaks at 2θ values 13.5°, 22°, and 39° were observed for sodium alginate due to polyguluronate unit, polymannuronate, and the other from amorphous halo.

LMP outline peaks in XRD spectra at angles $2\theta = 13.38°$ and 20.87° as similar as XRD patterns of SA (Fig. 4). The spectrum of LMP indicated that the crystallinity of the galacturonic acid of pectin. A similar finding was reported by Zykwinska, A., (2007), who suggested

that the spectrum of galacturonic acid of pectin revealed two principal Bragg reflections, at 12.6° and 20.4°.

The diffraction pattern of curcumin compound appeared a crystalline in nature, as it shows multiple peaks at angles 2θ = 9.02°, 12.29°, 14.62°, 17.44°, 18.28°, 19.54°, 21.34°, 23.53°, 23.96°, 24.65°, 25.69°, 26.18°, 27.47°, and 29.08°. J. Su et al., (2021) also indicated that pure curcumin was found to be in a crystalline state, verified by the presence of diffraction peaks at angles of 12.3°, 14.6°, 17.3°, 21.2°, and 29.1°.

CS and $CaCl_2$ which made up the cross-linking solution showed a peaks in XRD spectra at angles 2θ = 9.98°, 19.97°, and at angles 2θ = 14.67°, 20.58°, 21.11°, 29.54°, 31.99°, 34.14°, 38.22°, and 42.82°, respectively, indicating the crystalline behavior.

It is clear that the one broad peak was shown in XRD pattern of (1:1) IG solution (sol.) powder, mixing with (1:1) of SA and LMP and inducing internal gelation (IG) before drying, at 15.50° (Fig. 5). The result suggested that with internal egg-box structure, the suspension (weak-gel) exhibited more regular and homogeneous arrangement compared to the other powders, resulting in one broad peak. In other words, the formation of egg-box structure through IG showed

monodispersed structure of the sample with IG. Also, in the (1:1) suspension with IG (Fig. 5), increase in crystallinity at 15.50° was seen as compared to (1:1) suspension. The crystallinity degree at 15.50° increased with formation of egg-box structure through IG. The increasing crystallinity degree of (1:1) IG suspension exhibited that the presence of physical cross-linking, resulting in new crystalline phases. S. Hua et al., (2010) reported the similar results, indicating that the crystallinity degree of dried gel beads increased after the treatment of FT which may be due to the formation of physical crosslinking points.

According to the XRD pattern of all the beads, there are broad absorption peaks, indicating that the beads had amorphous structures. Moreover, the XRD spectrum of the beads exhibited the disappearance of curcumin spectral lines. The crystalline peaks of curcumin were absent in the beads containing curcumin. This indicated that the curcumin was not in crystalline form after entrapment, and CS-SA/LMP beads for curcumin had a remarkable encapsulation capacity. The core substance, curcumin, had been encapsulated or dispersed well into SA/LMP polymers, subsequently forming an amorphous complex. The similar results could be seen in A. Patel, (2010), who suggested that the XRD diffractogram of zein-curcumin colloidal particles showed

complete disappearance of the characteristic crystalline peaks of curcumin due to the formation of an amorphous complex with zein within the particle matrix. Moreover, Moumita, H., (2015) also reported that the molecule of quercetin had been successfully entrapped or dispersed into chitosan–alginate polymers when undergoing the ionic cross-linking technique, thus forming an amorphous complex with intermolecular interaction occurring within the matrix. Therefore, there is no characteristic peaks appearing on the patterns of the formulation.

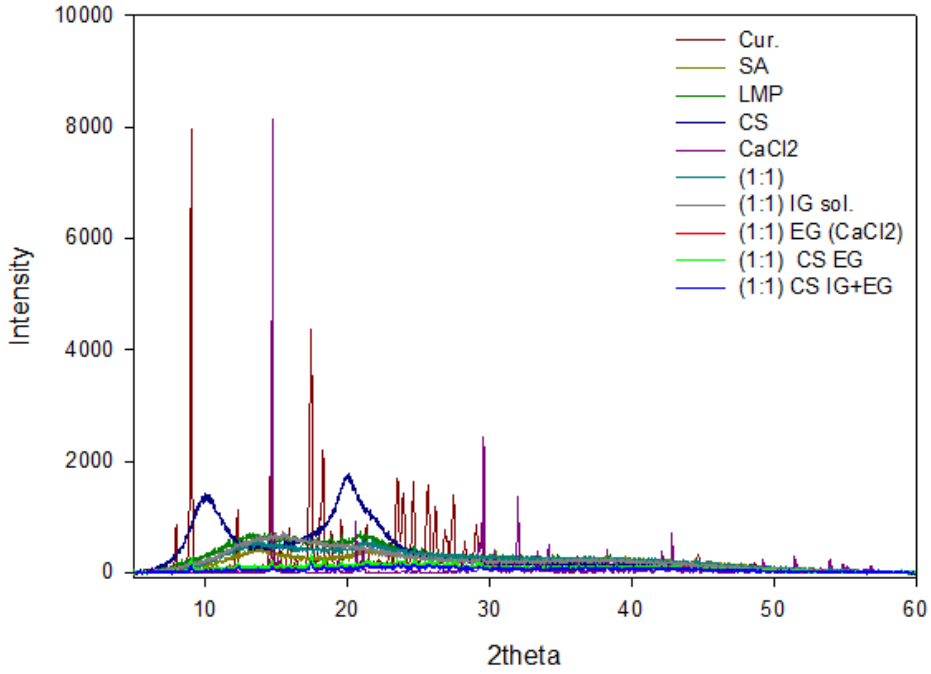

Figure 3. X-ray diffraction (XRD) patterns of the materials.

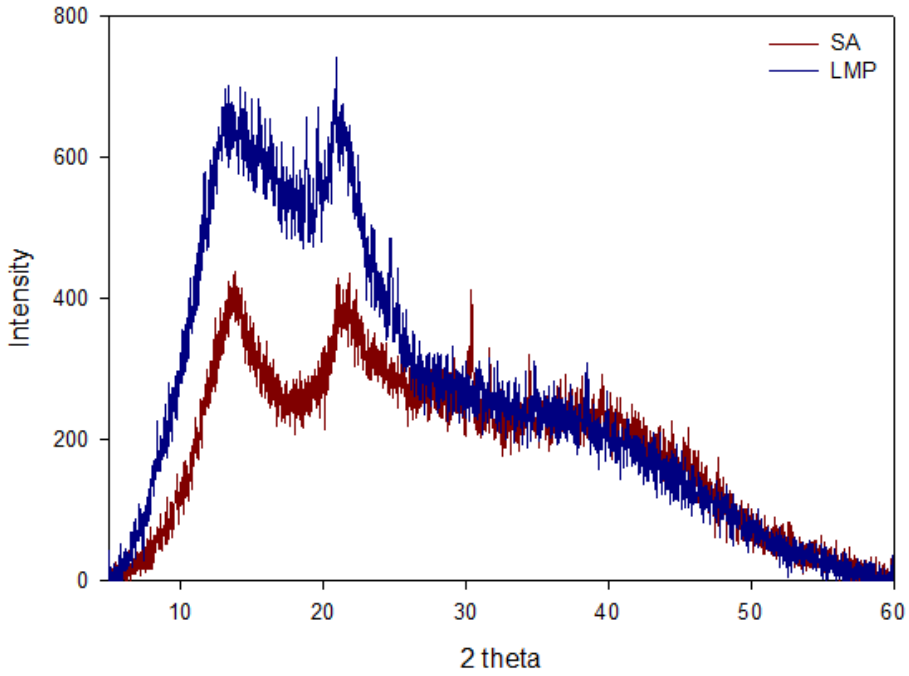

Figure 4. X-ray diffraction (XRD) patterns of sodium alginate (SA) and low methoxyl pectin (LMP).

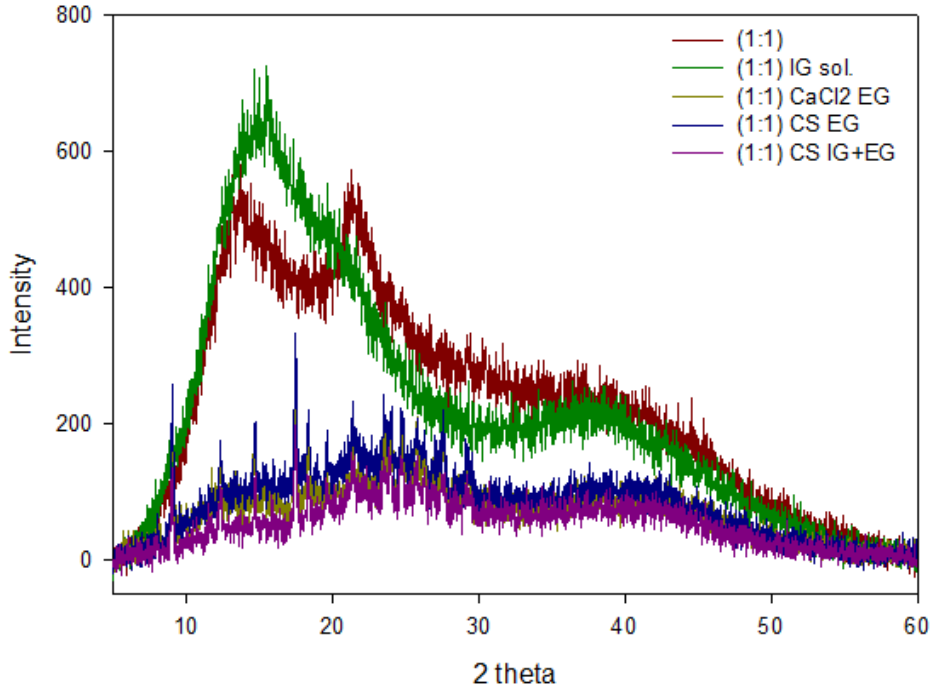

Figure 5. X-ray diffraction (XRD) patterns of the suspension and beads with (1:1) of SA/LMP depending on the presence of internal gelation (IG).

3.5. Fourier transform infrared (FTIR) spectroscopy

The vibrational frequencies related to specific chemical groups are recorded in specific IR regions, which depend on the type of both chemical bonds and atoms involved (Hamed H., Seid M.J., 2020). The FTIR spectra of materials are indicated in Fig. 6 and Fig. 7.

The blended powder of (1:1) exhibited a characteristic peak at 3380 cm^{-1}, which was ascribed to the stretching of OH groups, while the peak of the 3 types of (1:1) beads shifted to the lower band of 3330-3333 cm^{-1}, indicating the enhanced hydrogen bond interactions (X.Yang et al., 2018; Wang, D. Zhao, K., 2016). The stronger hydrogen bonding concomitantly increased the hydrophilic interactions (M. Ahmadi, A. Madadlou, 2016).

The peaks of SA at 1604, LMP at 1612, and (1:1) powder and (1:1) IG at 1606, respectively, were shifted to 1601-1602 of (1:1) beads, indicating that carboxyl groups ($-COO^-$) of SA/LMP were cross-linked with Ca^{2+} (T. Lee, Y.H. Chang, 2020). The bands observed at 1408-1412 in SA, LMP, (1:1) powder, and (1:1) sol. were shifted to about 1429 in 3 types of (1:1) beads. This is because crosslinking between COO^- and $Ca^{2+,}$ and polyelectrolyte complex between COO^- and NH_3^+ were formed in the beads. The similar results reported by (Lawrie et al., 2007; Simsek-

Ege et al., 2003) proposing that the band observed at 1420 cm^{-1} in 1:1 alginate-chitosan mixtures was due to the interaction of $–NH_3^+$ (from chitosan) with $–COO^-$ (from alginate and pectin).

The FTIR spectrum of curcumin showed the presence of characteristic functional groups at 1155, 1280, 1508, 1602, and 1628 corresponding to the CCH of aromatic rings, CH of C=CH, C=O and CC=O, C=C of aromatic rings, and C=O and C=C of the interring chain, respectively (C.S. Mangolim, 2014). The 3 types of beads showed the characteristic peaks of curcumin at about 1155, 1281, 1509, 1602, and 1627 which were associated with CCH of aromatic rings, CH of C=CH, C=O and CC=O, C=C of aromatic rings, and C=O and C=C of the interring chain, respectively (C.S. Mangolim, 2014), indicating that the beads encapsulated curcumin. These spectrums representing the chemical groups were not detected in the other samples of FT-IR.

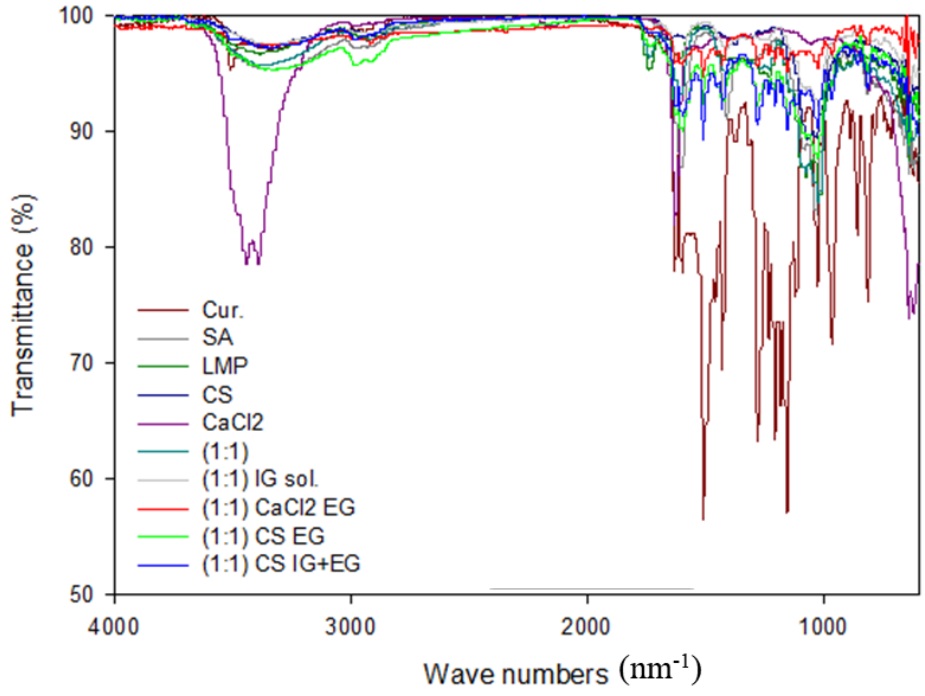

Figure 6. Fourier transform infrared (FTIR) spectroscopy of materials.

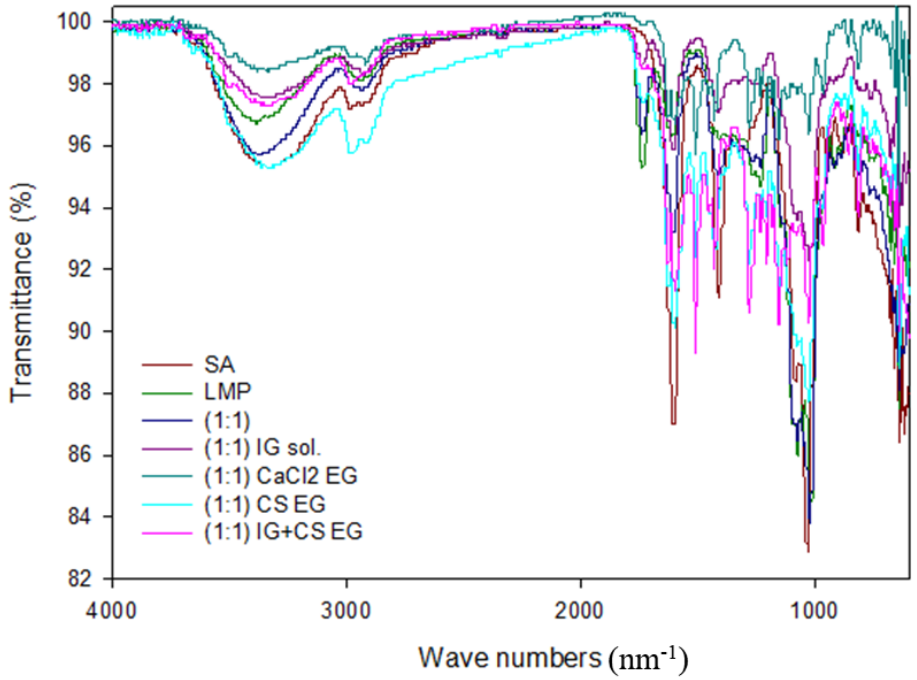

Figure 7. Fourier transform infrared (FTIR) spectroscopy of materials and the suspension and beads with (1:1) of SA/LMP depending on the presence of internal gelation (IG) and CS-coating.

3.6. Scanning electron microscopy (SEM)

The microstructures of lyophilized beads were confirmed by SEM. Fig. 8. showed microstructure of the beads depending on different blend proportions of SA/LMP, the presence of egg-box structure through IG, and the presence of CS-coating. In the case of the control groups with SA, the SA beads formed the thicker and stronger wall, and comparatively ordered structure (Fig. 8). On the other hand, the pore distribution of LMP beads have thinner and fluffy structure (Fig. 8). The LMP beads also showed thin and raggered inner structure, resulting in weaker textural properties (Table. 2). Irregularly inner structures were developed with thin and smaller sizes of holes. Consequently, the higher the SA ratio of SA/LMP beads, the stronger the textural properties (Table. 2), because the wall of SA is thicker and stronger than LMP. Unlike more regular structures were shown in SA, the lopsided structure in LMP beads due to its randomized methylesterification of galacturonate units. Thus, the LMP beads would be cross-linked lopsidedly, which resulted in huge cavities in the complexes. The result is because the beads which has methoxyl groups in galacturonic acid of LMP had relatively low calcium-sensitivity. The methoxyl groups of LMP prefer to be distributed in block-wise manner which would hinder the crosslink between COO^-

and Ca^{2+}. Therefore, LMP with fewer carboxyl groups might develop the lopsided structure, and showed poly-dispersed and disordered pores.

The beads obtained by both core crosslinking and surface crosslinking (Fig. 8 (B), (D), (J)) appeared compact and denser structure, compared to the beads composed of the same blend proportions of SA/LMP and formed only by surface crosslinking. Besides, the beads with both IG and EG appeared more regular structure and monodispersed distribution of pores. The microstructures were correlated to the results of XRD (Fig. 5), indicating that the suspension with IG had more regular and homogeneous arrangement compared to the suspension without IG. Especially, there are clear differences between Fig. 8 (A) and (B), and Fig. 7 (I) and (J). Compared to the Fig. 8 (A) and (B) showed evidently smaller and finer structures. Moreover, the beads induced by IG (Fig. 8 (N)) appeared no huge cavities and more massed pores different from the beads only induced by EG (Fig. 8 (M)).

The denser structure of the beads with IG was originated from chemical crosslinking between carboxyl groups of SA/LMP and calcium ions, resulting in physical crosslinking. In other words, the carboxylate groups of SA/LMP cross-linked with Ca^{2+} to form egg-box structure through IG, in place of more ionic-interaction with CS and crosslinking

with Ca^{2+} on the bead surface through EG. Finally, the beads with both IG and EG exhibited more compact structure, but softer texture than only with EG, although there is no significant difference (Table. 2).

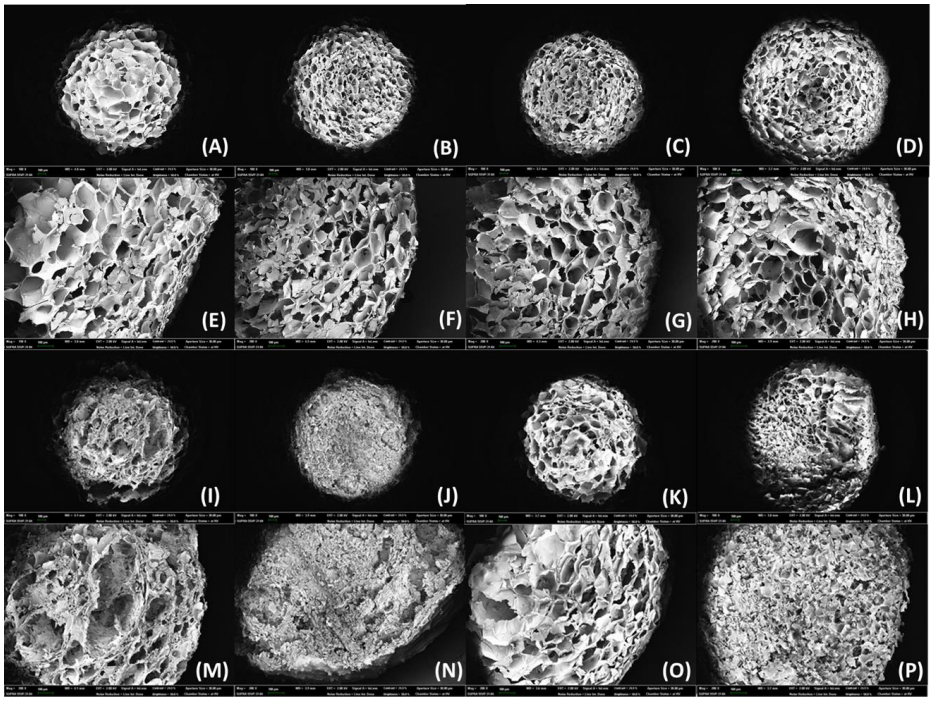

Figure 8. Scanning electron microscopy (SEM) images of lyophilized beads with different blend ratio of SA/LMP depending on the presence of internal gelation (IG) including (A) (2:1) EG (B) (2:1) IG (C) (1:1) EG (D) (1:1) IG (I) (1:2) EG (J) (1:2) IG (K) SA EG (L) LMP EG. Samples were shown at magnification of 100 × (first and third lines) and 200 × (second and forth lines).

3.7. Releasing behavior

The releasing behavior test was conducted to observe the release patterns of each sample (Fig. 9). In gastric pH, $–COO^–$ groups of SA/LMP were protonated and became hydrophobic (COOH), subsequently the beads could prevent water diffusion more effectively (A. Abbaszad, 2015). Therefore, the release of beads in gastric pH rarely occurred. However, $–NH_2$ groups of CS were also protonated and became hydrophilic ($–NH_3^+$), subsequently the beads could be soluble in acid pH and swelling. Therefore, the thick swollen layer of CS in acid pH was formed as a role of diffusion barrier layer.

When the beads were exposed to neutral pH of small and large intestine, there appeared to be an increase in turbidity of the fluid, indicating that the beads were hydrolyzed by phosphate ions in PBS (small and large intestinal fluid) and pectinase in large intestinal fluid. In other words, when the beads were transferred into medium of above pH 3.3-3.6, the pKa value of SA/LMP, the –COOH group begin to ionize to give $–COO^-$ charged groups and there may start very slow ion-exchange between Ca^{2+} ions, thus resulting in decrease in degree of crosslinking and greater uptake of water (S.K. Bajpai, 2004). SA/LMP dissolved when exposed to higher pH than pKa (Pawar, S.N., 2012; Rehm, 2009).

The remained curcumin of the beads in small intestinal pH would be delivered to colon and then released from the pectinate beads decomposed by colonic microflora producing pectinolytic enzymes (Zhang et al., 2016; Matalanis et al., 2011). Moreover, the beads containing LMP destroyed significantly in large intestinal fluid due to the degradation of the LMP by bacterial enzyme pectinase. The enzymatic erosion of the beads by pectinase appeared in large intestinal fluid.

The SA beads represented burst release 2 h after exposure to the small intestinal pH (Fig. 9). This is because SA contained more carboxylate groups, which could interact with Ca^{2+} and NH_3^+ of CS than LMP. The carboxylate groups showed stronger affinity with phosphate ions in neutral pH (pH of small and large intestine), resulting in the disintegration and erosion of complexes due to chelating effect of phosphate ions (A. Abbaszad, 2015). The phosphate ions in the medium captures the calcium ions inducing a fast disintegration of calcium-bead structure (Dhalleine et al., 2011). However, there are more carboxylate groups in SA, thus the substitution occurred slowly and so did the decomposition of the beads. Also, the thicker structure of SA (Fig. 8 (K)) tended to prevent the water release from the beads well and SA beads

were coated with CS, thus the slower diffusion of water and leaking of curcumin from the beads compared to LMP. However, burst release of SA beads appeared immediately after delay due to large porosity of SA. The SA beads without LMP exhibited the tendency to release from small intestinal pH and simulated large intestine fluid was not different and occurred continuously. Whereas, the LMP beads could not effectively prevent water absorption in gastric pH, because of LMP composed of lower amount of carboxylic acid. Also, the beads destroyed with weak textural properties, resulting in 21% release of curcumin in gastric pH.

Except control groups, especially LMP beads, the (1:1) beads which were cross-linked only with calcium ions without CS-coating released 3% of curcumin in gastric pH by the diffusion of water swollen and curcumin. This showed that the coating of CS polymer was protonated in gastric pH to represent NH_3^+, therefore only the CS absorbed water, serving as a water diffusion barrier. Finally, CS polymer coating could enhance protection of curcumin releasing in gastric pH.

In the case of comparing release patterns depending on the blend ratio of SA/LMP (Fig. 10), the beads with relatively higher SA and lower LMP like (2:1) beads showed slower release of curcumin. This is attributed to the fact that the substitution of the phosphate ions occurred

more slowly, resulting in slower release of curcumin. Moreover, the (2:1) beads composed of relatively lower amount of LMP would not occur severe burst release due to decomposition by pectinase, and the beads were affected by both neutral pH and pectinase gradually.

The beads with IG showed more uniform and denser wall distribution which could induce stronger structure (Fig. 8 (B), (D), (J)). The stronger structure could hold more water and prevent the water release from the beads with the impact of a stronger capillary force. Therefore, the egg-box structure of the beads formed by both IG and EG indicated more sustained release of curcumin compared to the beads which were composed of same blend ratio of SA/LMP and formed by only EG (Fig. 10). The monodispersed and finer structures also acted as a diffusion barrier of curcumin. As a result, the structure could be slowly affected by pectinase in large intestinal fluid, causing no rapid release of curcumin. Especially, in the case of (2:1) IG beads, it was the strongest structure which showed thick and dense structure. The structure of the beads led to the most sustained release of curcumin in colon. The increased beads density may also result in making the ion-exchange process lower and delayed degradation. The (2:1) EG beads released 29% of curcumin in small intestinal pH and 80% in large intestinal fluid in 2

h. Whereas, when the (2:1) IG beads were exposed to large intestinal fluid for 5 h, 80% of curcumin was released from the beads, and only 19% in small intestinal pH. The formation of egg-box structure through IG was related to the slower enetration of the enzyme into the beads, so that the beads were hydrolyzed more slowly.

Controlling both the degree of IG and blending proportions of SA/LMP, and coating of CS through polyelectrolyte complex have significant impact on the sustained release of curcumin in CS-coated SA/LMP beads. Consequently, the formulation designs applied to the beads have potential as curcumin delivery systems in the colon.

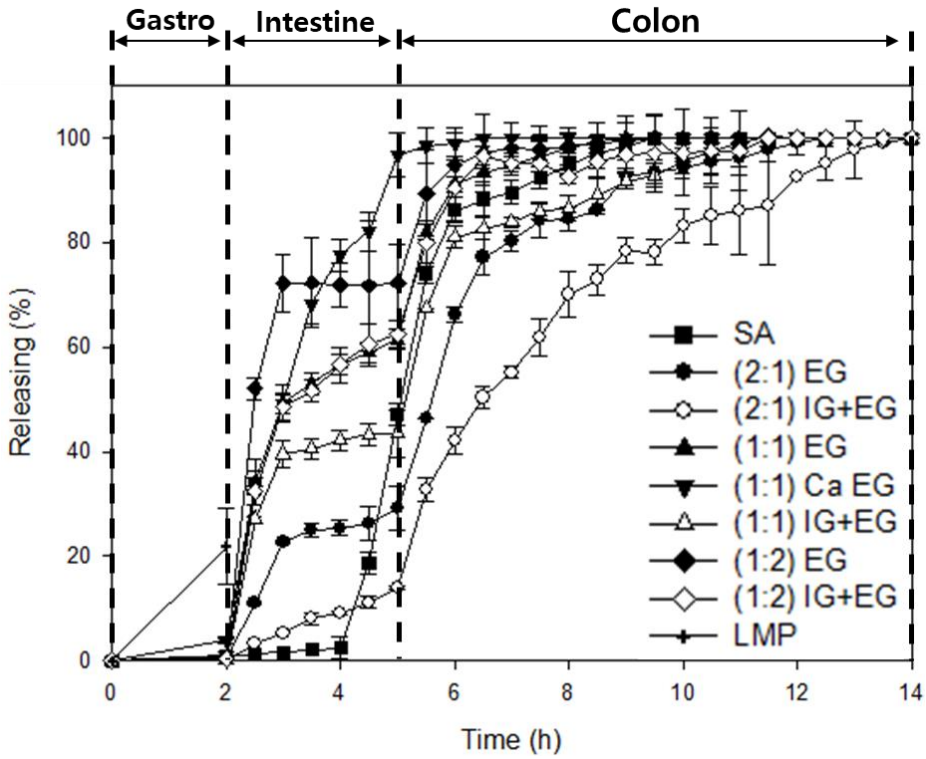

Figure 9. Releasing behaviors of the beads with different blend ratio of SA/LMP depending on the presence of internal gelation (IG) and CS-coating.

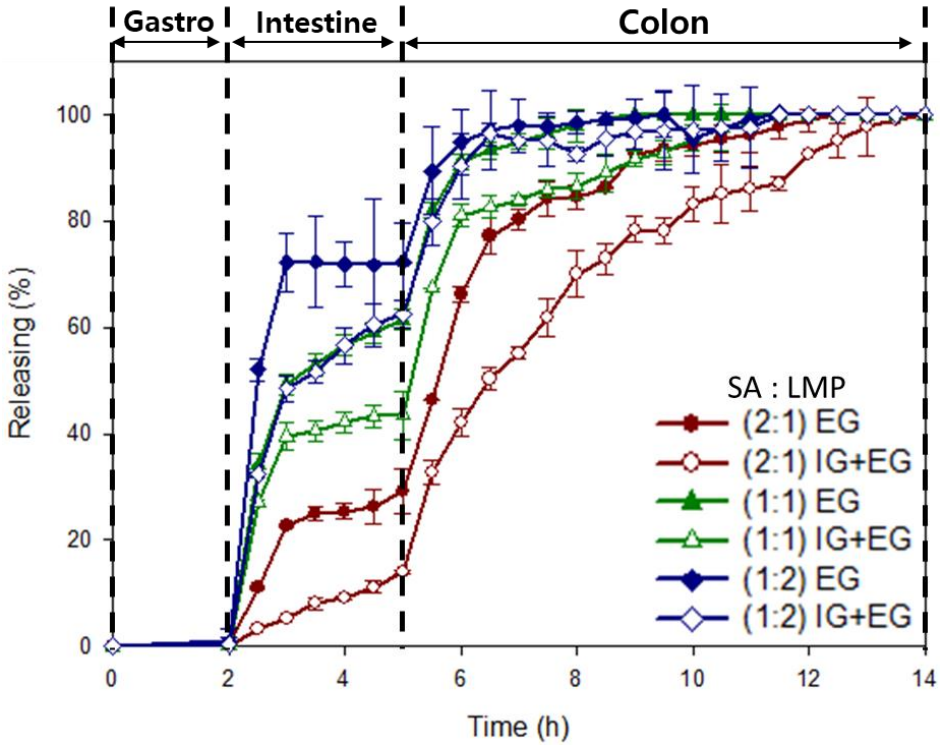

Figure 10. Releasing behaviors of the beads with different blend ratio of SA/LMP depending on the presence of internal gelation (IG) and CS-coating.

IV. Conclusions

In this study, the CS-coated SA/LMP beads which formed egg-box structure through internal gelation (IG) was used as a colon-specific curcumin delivery system. Based on XRD analysis, it was found that the formation of egg-box structure through IG caused more uniform and monodispersed structure. The FTIR result confirmed the cross-linking between carboxylic acid of SA/LMP and calcium ions, and the polyelectrolyte complex between carboxylic acid of SA/LMP and NH_3^+ of CS. The curcumin releasing studies showed the beads were stable in gastric pH, and they were dissolved in small intestinal pH due to higher pKa, and degraded by pectinase in large intestinal pH. The compact and uniform structures of the beads with IG prevented severe burst release in small intestinal pH and induced sustained release in large intestinal pH. The releasing of curcumin was controlled by the presence of IG, blend proportions of SA/LMP, and CS-coating. These results would widen the production of colon-targeted delivery systems for use in the functional food industry and also in cosmetic industry by controlling the degree of IG and CS-coating.

V. References

Ahmadi, M., Madadlou, A., & Saboury, A. A. (2016). Whey protein aerogel as blended with cellulose crystalline particles or loaded with fish oil. *Food chemistry*, *196*, 1016-1022.

Apoorva, A., Rameshbabu, A. P., Dasgupta, S., Dhara, S., & Padmavati, M. (2020). Novel pH-sensitive alginate hydrogel delivery system reinforced with gum tragacanth for intestinal targeting of nutraceuticals. *International journal of biological macromolecules*, *147*, 675-687.

Bajpai, S. K., & Sharma, S. (2004). Investigation of swelling/degradation behaviour of alginate beads crosslinked with Ca2+ and Ba2+ ions. *Reactive and Functional Polymers*, *59*(2), 129-140.

B. B. Patel and A. P. (2009). Majumdar, *Nutr. Cancer*, *61*, 842–846.

Braccini, I., & Pérez, S. (2001). Molecular basis of Ca2+-induced gelation in alginates and pectins: the egg-box model revisited. *Biomacromolecules*, *2*(4), 1089-1096.

Brahatheeswaran, D., Mathew, A., Aswathy, R. G., Nagaoka, Y., Venugopal, K., Yoshida, Y., ... & Sakthikumar, D. (2012). Hybrid fluorescent curcumin loaded zein electrospun

nanofibrous scaffold for biomedical applications. *Biomedical Materials*, *7*(4), 045001.

Cao, L., Lu, W., Mata, A., Nishinari, K., & Fang, Y. (2020). Egg-box model-based gelation of alginate and pectin: A review. *Carbohydrate polymers*, 116389.

Chen, K., & Zhang, H. (2019). Alginate/pectin aerogel microspheres for controlled release of proanthocyanidins. *International journal of biological macromolecules*, *136*, 936-943.

Dafe, A., Etemadi, H., Dilmaghani, A., & Mahdavinia, G. R. (2017). Investigation of pectin/starch hydrogel as a carrier for oral delivery of probiotic bacteria. *International journal of biological macromolecules*, *97*, 536-543.

Das, R. K., Kasoju, N., & Bora, U. (2010). Encapsulation of curcumin in alginate-chitosan-pluronic composite nanoparticles for delivery to cancer cells. *Nanomedicine: Nanotechnology, Biology and Medicine*, *6*(1), 153-160.

Dhalleine, C., Assifaoui, A., Moulari, B., Pellequer, Y., Cayot, P., Lamprecht, A., & Chambin, O. (2011). Zinc-pectinate beads as an in vivo self-assembling system for pulsatile drug delivery. *International journal of pharmaceutics*, *414*(1-2), 28-34.

Fan, L., Ge, H., Zou, S., Xiao, Y., Wen, H., Li, Y., ... & Nie, M. (2016). Sodium alginate conjugated graphene oxide as a new carrier for drug delivery system. *International journal of biological macromolecules*, *93*, 582-590.

Fang, D., Liu, Y., Jiang, S., Nie, J., & Ma, G. (2011). Effect of intermolecular interaction on electrospinning of sodium alginate. *Carbohydrate Polymers*, *85*(1), 276-279.

Fang, Y., Al-Assaf, S., Phillips, G. O., Nishinari, K., Funami, T., Williams, P. A., & Li, L. (2007). Multiple steps and critical behaviors of the binding of calcium to alginate. *The Journal of Physical Chemistry B*, *111*(10), 2456-2462.

Feng, K., Wei, Y. S., Hu, T. G., Linhardt, R. J., Zong, M. H., & Wu, H. (2020). Colon-targeted delivery systems for nutraceuticals: A review of current vehicles, evaluation methods and future prospects. *Trends in Food Science & Technology*.

Gaw³owski, A. (2005). Supermolecular Structure of Alginate Fibres for Medical Aplications Studied by Means of WAXS and SAXS Methods. *Fibres & Textiles in Eastern Europe*, *13*(5), 53.

George, M., & Abraham, T. E. (2006). Polyionic hydrocolloids for the intestinal delivery of protein drugs: alginate and chitosan—a review. *Journal of controlled release*, *114*(1), 1-14.

Günter, E. A., & Popeyko, O. V. (2016). Calcium pectinate gel beads obtained from callus cultures pectins as promising systems for colon-targeted drug delivery. *Carbohydrate polymers*, *147*, 490-499.

Hazra, M., Mandal, D. D., Mandal, T., Bhuniya, S., & Ghosh, M. (2015). Designing polymeric microparticulate drug delivery system for hydrophobic drug quercetin. *Saudi pharmaceutical journal*, *23*(4), 429-436.

Hosseini, H., & Jafari, S. M. (2020). Fourier transform infrared (FT-IR) spectroscopy of nanoencapsulated food ingredients. In *Characterization of Nanoencapsulated Food Ingredients* (pp. 347-410). Academic Press.

Hsu, F. Y., Yu, D. S., & Huang, C. C. (2013). Development of pH-sensitive pectinate/alginate microspheres for colon drug delivery. *Journal of Materials Science: Materials in Medicine*, *24*(2), 317-323.

Hua, S., Ma, H., Li, X., Yang, H., & Wang, A. (2010). pH-sensitive sodium alginate/poly (vinyl alcohol) hydrogel beads prepared by combined Ca2+ crosslinking and freeze-thawing cycles for controlled release of diclofenac sodium. *International journal of biological macromolecules*, *46*(5), 517-523.

Huanbutta, K., Cheewatanakornkool, K., Terada, K., Nunthanid, J., & Sriamornsak, P. (2013). Impact of salt form and molecular weight of chitosan on swelling and drug release from chitosan matrix tablets. *Carbohydrate polymers*, *97*(1), 26-33.

Jantrawut, P., Assifaoui, A., & Chambin, O. (2013). Influence of low methoxyl pectin gel textures and in vitro release of rutin from calcium pectinate beads. *Carbohydrate polymers*, *97*(2), 335-342.

Javanbakht, S., Nazari, N., Rakhshaei, R., & Namazi, H. (2018). Cu-crosslinked carboxymethylcellulose/naproxen/graphene quantum dot nanocomposite hydrogel beads for naproxen oral delivery. *Carbohydrate polymers*, *195*, 453-459.

Jeddi, M. K., & Mahkam, M. (2019). Magnetic nano carboxymethyl cellulose-alginate/chitosan hydrogel beads as biodegradable

devices for controlled drug delivery. *International journal of biological macromolecules*, *135*, 829-838.

Kaity, S., Isaac, J., & Ghosh, A. (2013). Interpenetrating polymer network of locust bean gum-poly (vinyl alcohol) for controlled release drug delivery. *Carbohydrate polymers*, *94*(1), 456-467.

Kaya, M. (2017). Super absorbent, light, and highly flame retardant cellulose-based aerogel crosslinked with citric acid. *Journal of Applied Polymer Science*, *134*(38), 45315.

Lawrie, G., Keen, I., Drew, B., Chandler-Temple, A., Rintoul, L., Fredericks, P., & Grøndahl, L. (2007). Interactions between alginate and chitosan biopolymers characterized using FTIR and XPS. *Biomacromolecules*, *8*(8), 2533-2541.

Malik, N. S., Ahmad, M., & Minhas, M. U. (2017). Cross-linked β-cyclodextrin and carboxymethyl cellulose hydrogels for controlled drug delivery of acyclovir. *PloS one*, *12*(2), e0172727.

Martău, G. A., Mihai, M., & Vodnar, D. C. (2019). The use of chitosan, alginate, and pectin in the biomedical and food sector—biocompatibility, bioadhesiveness, and biodegradability. *Polymers*, *11*(11), 1837.

Layek, B., & Mandal, S. (2020). Natural polysaccharides for controlled delivery of oral therapeutics: a recent update. *Carbohydrate polymers*, *230*, 115617.

Lee, C. H., Nalluri, L. P., & Popuri, S. R. (2019). Optimization studies for encapsulation and controlled release of curcumin drug using Zn+ 2 cross-linked alginate and carboxy methylcellulose blend. *Journal of Polymer Research*, *26*(1), 1-17.

Lee, K. Y., & Mooney, D. J. (2012). Alginate: properties and biomedical applications. *Progress in polymer science*, *37*(1), 106-126.

Lee, T., & Chang, Y. H. (2020). Structural, physicochemical, and in-vitro release properties of hydrogel beads produced by oligochitosan and de-esterified pectin from yuzu (Citrus junos) peel as a quercetin delivery system for colon target. *Food Hydrocolloids*, *108*, 106086.

Li, J., Kim, S. Y., Chen, X., & Park, H. J. (2016). Calcium-alginate beads loaded with gallic acid: Preparation and characterization. *LWT-Food Science and Technology*, *68*, 667-673.

Mangolim, C. S., Moriwaki, C., Nogueira, A. C., Sato, F., Baesso, M. L., Neto, A. M., & Matioli, G. (2014). Curcumin–β-cyclodextrin

inclusion complex: stability, solubility, characterisation by FT-IR, FT-Raman, X-ray diffraction and photoacoustic spectroscopy, and food application. *Food chemistry*, *153*, 361-370.

Matalanis, A., Jones, O. G., & McClements, D. J. (2011). Structured biopolymer-based delivery systems for encapsulation, protection, and release of lipophilic compounds. *Food Hydrocolloids*, *25*(8), 1865-1880.

Nguyen, A. T. B., Winckler, P., Loison, P., Wache, Y., & Chambin, O. (2014). Physico-chemical state influences in vitro release profile of curcumin from pectin beads. *Colloids and Surfaces B: Biointerfaces*, *121*, 290-298.

Pan, M. K., Zhou, F. F., Liu, Y., & Wang, J. H. (2021). Na+-induced gelation of a low-methoxyl pectin extracted from Premna microphylla Turcz. *Food Hydrocolloids*, *110*, 106153.

Patel, A., Hu, Y., Tiwari, J. K., & Velikov, K. P. (2010). Synthesis and characterisation of zein–curcumin colloidal particles. *Soft Matter*, *6*(24), 6192-6199.

Pawar, A., Gadhe, A., Venkatachalam, P., Sher, P., & Mahadik, K. (2008). Effect of core and surface cross-linking on the

entrapment of metronidazole in pectin beads. *Acta Pharmaceutica*, *58*(1), 78.

Pawar, S. N., & Edgar, K. J. (2012). Alginate derivatization: a review of chemistry, properties and applications. *Biomaterials*, *33*(11), 3279-3305.

Prezotti, F. G., Cury, B. S. F., & Evangelista, R. C. (2014). Mucoadhesive beads of gellan gum/pectin intended to controlled delivery of drugs. *Carbohydrate polymers*, *113*, 286-295.

Rajmohan, D., & Bellmer, D. (2019). Characterization of Spirulina-alginate beads formed using ionic gelation. *International journal of food science*, *2019*.

Rafi, A. A., & Mahkam, M. (2015). Preparation of magnetic pH-sensitive microcapsules with an alginate base as colon specific drug delivery systems through an entirely green route. *RSC advances*, *5*(6), 4628-4638.

Rehm, B.H.A. Alginates: Biology and Applications; Springer: Berlin/Heidelberg, Germany, 2009; ISBN 978-3-540-92678-8.

Riyajan, S. A., & Nuim, J. (2013). Interaction of green polymer blend of modified sodium alginate and carboxylmethyl cellulose

encapsulation of turmeric extract. *International Journal of Polymer Science*, *2013*.

Sampaio, G. L., Pacheco, S., Ribeiro, A. P. O., Galdeano, M. C., Gomes, F. S., & Tonon, R. V. (2019). Encapsulation of a lycopene-rich watermelon concentrate in alginate and pectin beads: Characterization and stability. *LWT*, *116*, 108589.

Sattarahmady, N., Moosavi-Movahedi, A. A., Bazzi, P., Heli, H., & Pourtakdoust, S. (2016). Improving pharmaceutical characteristics of curcumin by alginate/pectin microparticles. *Pharmaceutical Chemistry Journal*, *50*(3), 131-136.

Simsek-Ege, F. A., Bond, G. M., & Stringer, J. (2003). Polyelectrolyte complex formation between alginate and chitosan as a function of pH. *Journal of Applied Polymer Science*, *88*(2), 346-351.

Sookkasem, A., Chatpun, S., Yuenyongsawad, S., & Wiwattanapatapee, R. (2015). Alginate beads for colon specific delivery of self-emulsifying curcumin. *Journal of Drug Delivery Science and Technology*, *29*, 159-166.

Sriamornsak, P., Sungthongjeen, S., & Puttipipatkhachorn, S. (2007). Use of pectin as a carrier for intragastric floating drug delivery: Carbonate salt contained beads. *Carbohydrate Polymers*, *67*(3), 436-445.

Srinivasan, S., Jayasree, R., Chennazhi, K. P., Nair, S. V., & Jayakumar, R. (2012). Biocompatible alginate/nano bioactive glass ceramic composite scaffolds for periodontal tissue regeneration. *Carbohydrate Polymers*, *87*(1), 274-283.

Su, J., Cai, Y., Zhi, Z., Guo, Q., Mao, L., Gao, Y., ... & Van der Meeren, P. (2021). Assembly of propylene glycol alginate/β-lactoglobulin composite hydrogels induced by ethanol for co-delivery of probiotics and curcumin. *Carbohydrate Polymers*, *254*, 117446.

Ubeyitogullari, A., & Ciftci, O. N. (2016). Formation of nanoporous aerogels from wheat starch. *Carbohydrate polymers*, *147*, 125-132.

U.S. Department of Health and Human Services, Food and Drug Administration, Center for Drug Evaluation and Research (CDER), "Guidance for Industry Size of Beads in Drug Products Labeled for Sprinkle", 2012.

Wang, B., Gao, B., Zimmerman, A. R., Zheng, Y., & Lyu, H. (2018). Novel biochar-impregnated calcium alginate beads with improved water holding and nutrient retention properties. *Journal of environmental management*, *209*, 105-111.

Wang, H., Gong, X., Guo, X., Liu, C., Fan, Y. Y., Zhang, J., ... & Li, W. (2019). Characterization, release, and antioxidant activity of curcumin-loaded sodium alginate/ZnO hydrogel beads. *International journal of biological macromolecules*, *121*, 1118-1125.

Wang, J., Zhao, D., Shang, K., Wang, Y. T., Ye, D. D., Kang, A. H., ... & Wang, Y. Z. (2016). Ultrasoft gelatin aerogels for oil contaminant removal. *Journal of Materials Chemistry A*, *4*(24), 9381-9389.

Yang, X., Nisar, T., Liang, D., Hou, Y., Sun, L., & Guo, Y. (2018). Low methoxyl pectin gelation under alkaline conditions and its rheological properties: Using NaOH as a pH regulator. *Food Hydrocolloids*, *79*, 560-571.

Zhang, W., Mahuta, K. M., Mikulski, B. A., Harvestine, J. N., Crouse, J. Z., Lee, J. C., ... & Tritt, C. S. (2016). Novel pectin-based

carriers for colonic drug delivery. *Pharmaceutical development and technology*, *21*(1), 127-130.

Zhang, Y. Z., Venugopal, J., Huang, Z. M., Lim, C. T., & Ramakrishna, S. (2006). Crosslinking of the electrospun gelatin nanofibers. *Polymer*, *47*(8), 2911-2917.

Zhang, Z., Zhang, R., Zou, L., Chen, L., Ahmed, Y., Al Bishri, W., ... & McClements, D. J. (2016). Encapsulation of curcumin in polysaccharide-based hydrogel beads: Impact of bead type on lipid digestion and curcumin bioaccessibility. *Food Hydrocolloids*, *58*, 160-170.

Zou, Q., Zhao, J., Liu, X., Tian, F., Zhang, H. P., Zhang, H., & Chen, W. (2011). Microencapsulation of Bifidobacterium bifidum F-35 in reinforced alginate microspheres prepared by emulsification/internal gelation. *International journal of food science & technology*, *46*(8), 1672-1678.

Zykwinska, A., Gaillard, C., Buléon, A., Pontoire, B., Garnier, C., Thibault, J. F., & Ralet, M. C. (2007). Assessment of in vitro binding of isolated pectic domains to cellulose by adsorption isotherms, electron microscopy, and X-ray diffraction methods. *Biomacromolecules*, *8*(1), 223-232.

VI. 국문초록

기능성 물질 커큐민은 대장에서 항염증, 항암의 특징을 가져, 바이오 활성 물질, 기능성 식품, 의약품으로 이용된다. 하지만 낮은 수용성 및 안정성 때문에 낮은 경구 생체이용성을 가진다. 따라서 이를 극복하기 위해 소화 효소에 의해 분해되지 않으며 pH 에 따라 방출 양상이 다른 알긴산과 펙틴을 이용한 하이드로젤 환을 제조하여, 위와 소장에서 커큐민을 보호하고 대장에서 지속적인 방출을 유도했다. 알긴산의 큰 다공성과 펙틴의 약한 물성의 한계점으로, 각각을 단독 사용 시 약물이 급격히 방출된다. 따라서 알긴산과 펙틴을 혼합하여 물리적인 얽힘을 유도했고, 내부적 젤화로 내부에 달걀 상자 구조를 형성하여 구조를 균일하고 밀집되게 만들었다. 그리고 외부적 젤화를 통해 환 형태로 제조하기 위해 키토산과 칼슘을 이용했다. 알긴산-펙틴의 COO^-와 키토산의 NH_3^+의 이온결합, Ca^{2+}과의 가교결합을 통해 환으로 제조했으며, 키토산 코팅으로 수분 확산 장벽의 역할을 부여했다. 환은 TPA, XRD, FT-IR, SEM 을 통해 내부적 달걀 상자 구조의

형성으로 인해 구조가 더 일정한 배율로 밀집되어 결정도가 높아졌으며, 키토산과의 이온결합과 칼슘 이온과의 가교결합이 형성된 것을 확인했다. 위장의 pH 에 따른 커큐민의 방출 실험을 통해 하이드로젤 환은 위에서 안정적이고 소장과 대장에서는 높은 pH 에 의해 용해되며 대장에서는 펙티네이스에 의해 분해되는 것을 확인할 수 있었다. 내부적 젤화를 유도한 환의 보다 획일적이고 조밀한 구조는 소장에서 커큐민의 급격한 방출을 막고 대장에서 지속적인 방출을 유도했다. 알긴산과 펙틴을 2:1 로 혼합한 환의 경우, 외부적 젤화만 유도한 환은 소장에서 커큐민의 약 29%가 방출되고, 대장에서 2 시간만에 80%가 방출됐다. 내부적 및 외부적 젤화 모두 유도한 환은 소장에서 14%만 방출되고, 대장에서 5 시간 때 80%를 방출했다. 이를 통해 달걀 상자 구조의 형성이 소장에서 급격한 방출을 막으며, 대장에서 지속적인 방출을 유도함을 확인할 수 있었다. 또한 키토산 코팅의 유무에 따른 커큐민 방출을 비교했을 때, 코팅이 없는 환은 위에서도 약 3% 방출되지만, 코팅된 환은 전혀 방출되지 않았다. 따라서

커큐민 뿐만 아니라, 대장에 유용한 기능성을 가지는 다른 물질이나 유산균 등에도 내부적 달걀 상자 구조의 형성과 키토산 코팅의 구조 설계를 적용하여, 위와 소장에서 보호하며 대장에서 지속적인 방출을 유도할 수 있을 것이다.

주요어 : 하이드로젤 환, 알긴산, 저메톡실펙틴, 키토산 코팅, 내부적 젤화, 달걀 상자 구조, 외부적 젤화, 고분자전해질 복합체, 대장 타겟 방출

학번 : 2019-20409